Available online at www.sciencedirect.com
ScienceDirect
Journal of Nuclear Materials 363–365 (2007) 560–564
journal of nuclear materials
www.elsevier.com/locate/jnucmat

Kinetic calculation of plasma deposition in castellated tile gaps

R. Dejarnac [a,*], J.P. Gunn [b]

[a] Association EURATOM-IPP.CR, Prague, Czech Republic
[b] Association EURATOM-CEA, Centre de Cadarache, 13108 Saint Paul Lez Durance, France

Abstract

Plasma-facing divertors and limiters are armoured with castellated tiles to withstand intense heat fluxes. Recent experimental studies show that a non-negligible amount of deuterium is deposited in the gaps between tiles. We present here a numerical study of plasma deposition in this critical region. For this purpose we have developed a particle-in-cell code with realistic boundary conditions determined from kinetic calculations. We find a strong asymmetry of plasma deposition into the gaps. A significant fraction of the plasma influx is expelled from the gap to be deposited on the leading edge of the downstream tile.

PACS: 52.40.Hf; 52.55.Fa; 52.65.−y; 52.65.Rr

Keywords: Divertor plasma; Edge modeling; Ion–surface interactions; ITER; Sheaths

1. Introduction

In order to help the future vertical target of the ITER divertor to withstand strong thermomechanical stresses [1] due to intense, inhomogeneous particle and heat fluxes [1], its armour will be castellated, i.e., split into cells [2]. This will increase the exposed surface of the limiter. Plasma and charge exchanged neutrals will flow into the gaps where tritium can be trapped in deposited hydrocarbon layers. A recent experimental study in TEXTOR [3] has shown significant deposited layers in the gaps of an ITER-like castellated test-limiter. A minimum of 30% of the deuterium retained on the top surface of the tiles is found in the gaps. We present here a two-dimensional numerical study of plasma deposition inside the tile gaps. Our investigation is performed using a standard particle-in-cell (PIC) technique (Section 2). The novelty consists of the realistic boundary conditions that satisfy the kinetic Bohm criterion. The particle deposition with respect to the depth and the width of the gap for different inclinations of the magnetic field lines are performed and presented in Section 3. Two orientations of the incident toroidal magnetic field, parallel and perpendicular to the gap are investigated. Particle flow asymmetries occurring inside the gap are of particular interest. The physics of plasma flow through a small orifice or a hollow conductor is known [4] and

* Corresponding author. Address: Za Slovankou 3, 182 00 Prague 8, Czech Republic. Fax: +420 286 89 0448.
E-mail address: dejarnac@ipp.cas.cz (R. Dejarnac).

0022-3115/$ - see front matter © 2007 Elsevier B.V. All rights reserved.
doi:10.1016/j.jnucmat.2006.12.055

governs the plasma deposition inside the tile gaps. A summary of the results is presented and the conclusions drawn in Section 4.

2. Tile gap modeling

2.1. The two-dimensional kinetic model

The numerical tool we have developed for this study is a three velocity – two-dimensional kinetic code. The solution scheme is similar to the ones usually used in PIC code modeling and based on [5]. The case considered in this paper is a fully ionized magnetized plasma with one species of singly charged ions incident on a completely absorbing, conducting wall. The code is based on the resolution of the equations of motion and the integration of Poisson's equation [6] to obtain the self-consistent electric field that accelerates the particles. We solve the equations of motion for both species (electrons and ions) with an implicit leapfrog [7] integration method. The novelty of the code is its ability to inject arbitrary velocity distribution functions. For the ions, we use a non-Maxwellian distribution given by a one-dimensional quasineutral kinetic calculation of the scrape-off layer [8,9] that satisfies the kinetic Bohm criterion at the electrostatic sheath entrance. The injected electrons are assumed to be Maxwellian. At equilibrium the electric field decays to zero far from the tile surface with no formation of a numerical sheath near the particle injection plane.

2.2. Simulation description

The Cartesian coordinate system used for the PIC simulation is illustrated in Fig. 1. All gradients are zero in the ignorable x-direction and the system

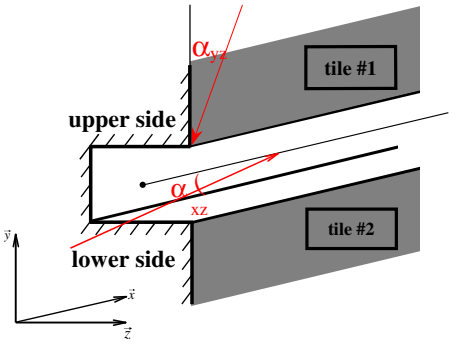

Fig. 1. Scheme of the simulation domain in Cartesian coordinates.

is periodic in y. The absorbing wall corresponding to the tiles #1 and #2 is set at the floating potential $V_0 \approx -3kT_e$ while the plasma side of the simulation is set at the potential $V_L = 0$. The uniform magnetic field can have an arbitrary orientation and is defined by two angles, α_{xz} and α_{yz}, corresponding to the projection of $\boldsymbol{B}$ into the planes (x–z) and (y–z), respectively. We inject ions (electrons) from the plasma side with the kinetic (Maxwellian) distribution in the parallel direction along $\boldsymbol{B}$. In the two other perpendicular directions, a Maxwellian distribution is assumed for both species. In the 1D case, when the $\boldsymbol{B}$ angle is oblique with an infinite surface, a magnetic sheath [10,11] develops in the range of $4r_L$, where r_L is the Larmor radius at the cold ion sound speed. This has been taken into consideration by enforcing a minimum distance of $10r_L$ in between the tiles surface and the plasma boundary in order to have no perturbation of the bulk plasma. The magnetic sheath can be parameterized by the factor $\zeta = r_L/\lambda_D$ [11]. In our simulations, we set $n_e = 2 \times 10^{18}\ \mathrm{m}^{-3}$, $T_e = 10\ \mathrm{eV}$, and $B = 5\ \mathrm{T}$, yielding $\zeta = 5$ to model a moderate flux zone with a partially magnetized sheath. These conditions are favourable for the growth of thick carbon deposits inside tile gaps in the Tore Supra tokamak. The length of the surface of the tiles in the y-direction is also taken large enough to avoid perturbations generated by the gap itself due to the periodicity of the system. We verify that the solution at the boundaries $y = 0$, $y = L_y$, is identical to the semi-infinite 1D solution.

We simulate two types of gaps according to their orientations with the magnetic field lines. Gaps parallel to the poloidal direction, i.e., $\boldsymbol{B}$ in the (y–z) plane ($\alpha_{xz} = 90°$), and parallel to the toroidal direction, i.e., $\boldsymbol{B}$ in the (x–z) plane ($\alpha_{yz} = 90°$), are called poloidal and toroidal gaps, respectively. In the following, we will only use the terms α and the gap orientation to describe the incident angle. In ITER, the vertical target will consist of castellated 10×10 mm tiles with a gap width of 0.5 mm. The incidence of the field lines should be at most 5°. We have investigated two angles, $\alpha = 5°$ and $\alpha = 20°$ (like in [3]) for both poloidal and toroidal gaps, as well as two different gap widths, $l_{gap} = 0.5$ mm and $l_{gap} = 1$ mm.

3. Results and discussion

We limit the present discussion to the particle fluxes only. Power fluxes follow the trend shown

by the particle fluxes, and will be analyzed in detail in another publication. For better understanding, we use the terms vertical and horizontal relative to the y- and z-directions, respectively. With the same convention, the two sides of the gap are named upper side and lower side. Finally, unless specified, we present here figures for the so-called reference case, i.e., 1 mm gap and a 20° angle.

3.1. Poloidal gaps

The electric potential distribution in the simulation region shows a strong positive peak inside the gap (Fig. 2(a)). This structure is due to the different degree of magnetization of ions and electrons. Electrons remained tied to the $\boldsymbol{B}$ lines, but ions can move freely in the horizontal direction due to their Larmor gyration and the polarization drift [11]. This leads to strong positive charge separation. Fig. 3(a) shows the vertical ion flux falling onto the two sides of the gap along the horizontal axis. This flux is normalized to the theoretical unperturbed flux that impinges on the tile far from the gap. Around 70% of the incident ion flux flows downwards on the wetted side of the gap. Some flux (only <1%) is collected on the magnetically shadowed upper side due to parallel flow reversal of the ions that just graze the edge of the upper tile and get reflected by the positive potential inside the gap. The missing incident flux is expelled from the gap by the charge separation field; they continue along field lines to be collected on the leading edge of the lower tile (Fig. 2(a)). If we reduce the gap width to 0.5 mm the trajectories are similar and only the flux on the lower side is decreased by a factor of two. Defining a decay length of the deposited flux as 1% of the maximum flux inside the gap, we find that the plasma is deposited within 0.40 mm and 0.52 mm for the upper and the lower side, respectively. It has to be noted that the geometric projection on the lower side of a 20° line passing by the upper corner is 0.36 mm. If we add one Larmor radius it covers the maximum range of 0.44 mm. The geometric effect of Larmor gyration is thus the main action that explains the wetted area on the lower side for poloidal gaps. Fig. 4(a) shows the ion flux perpendicular to the tile faces normalized by the theoretical 1D influx. The flux at the upper part of tile #1 and at the lower part of tile #2 is constant and corresponds to the influx injected from the plasma side. We observe in the gap interval a decrease of the horizontal flux which is compensated by an increase of the vertical flux in this area. Indeed, we observe a significant increase of the horizontal particle flux deposited on the leading edge of tile #2. This confirms that a non-negligible fraction of the ions flowing into the gap in the parallel direction is expelled by the charge separation potential to be deposited on the top surface of tile #2 within 1 mm.

In the ITER case ($l_{gap} = 0.5$ mm, $\alpha = 5°$), due to such a small incident angle, only few particles enter

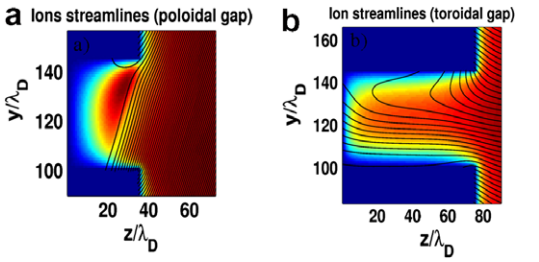

Fig. 2. Ion streamlines in the case of poloidal (a) and toroidal (b) gaps plotted over the electric potential normalized to kT_e/e for the reference case, i.e., an angle of 20° and a gap width of 1 mm.

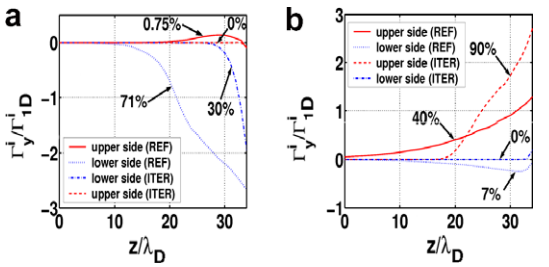

Fig. 3. Vertical ion flux falling on the sides of the gap for poloidal (a) and toroidal (b) cases normalized to the non-perturbed influx flowing onto tile surface far away from the gap for the reference case (20°, 1 mm). The ITER case (5°, 0.5 mm) is overplotted. The percentages correspond to the incident current normalized by the theoretical unperturbed current density at the gap entrance.

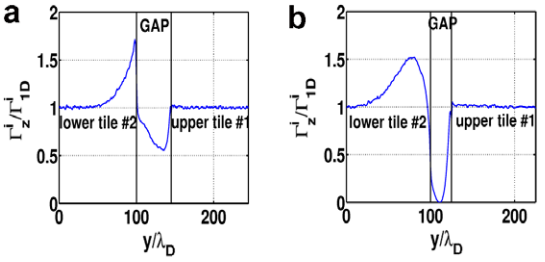

Fig. 4. Horizontal ion flux normalized to the non-perturbed influx flowing onto tile surface far away from the gap along the vertical coordinate at the gap entrance for a poloidal gap in the case of (a) reference (20°, 1 mm) and (b) ITER (5°, 0.5 mm).

the gap, therefore the particle flux deposited on the two sides on the gap is strongly reduced (Fig. 3(a)). No particles are collected by the upper side while 30% of the incident influx is found on the lower side. Decreasing the angle of incidence leads to an increase of the flux expulsion onto the lower tile #2 (Fig. 4(b)).

3.2. Toroidal gaps

In the case of toroidal gaps (Fig. 2(b)), there is a strong asymmetry in particle trajectories caused by the $\boldsymbol{E}\times\boldsymbol{B}$ drift in the magnetized sheath; at the tile surfaces this drift is directed upwards along the y-axis. Inside the gap, the $\boldsymbol{E}\times\boldsymbol{B}$ drift tends to sweep ions preferentially onto the upper surface. There, the drift can even cancel the incoming parallel flow, leading to a purely vertical flow onto the upper side of the gap. Fig. 3(b) shows that 40% of the influx is collected on the upper side of the gap and 7% on the lower side. The gap was not deep enough for the reference case of 20°, so a significant amount was also collected on the bottom of the gap (45%). Presumably this flux would go to the upper side if we had simulated a deeper gap. The missing flux (8%) is not expelled as in the case of poloidal gaps, but is lost before entry due to strong focusing of the electric field on the corner of the lower tile #2 (Fig. 5(a)). If we reduce the gap width to 0.5 mm, the trajectories are similar and again, only the values on the lower side are decreased by a factor of two.

In the ITER case ($l_{\mathrm{gap}} = 0.5$ mm, $\alpha = 5°$), we observe the same strong asymmetric deposition with no particles collected on the lower side (see Fig. 3(b)). Roughly, the same amount of influx is collected inside the gap (90% in this case compared to 92% in the reference case), but it is more concentrated near the gap entrance. In fact, practically no ions penetrate to the floor of the gap. This is due to the fact that the $\boldsymbol{E}\times\boldsymbol{B}$ drift dominates the horizontal projection of the parallel inflow for nearly grazing $\boldsymbol{B}$ angles.

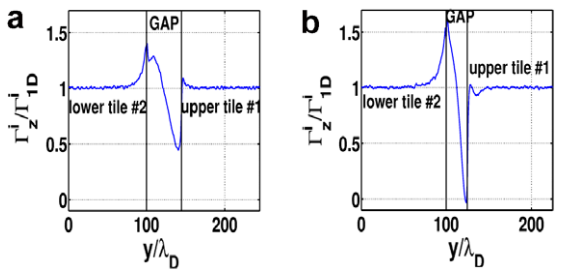

Fig. 5. Horizontal ion flux normalized to the non-perturbed influx flowing onto tile surface far away from the gap along the vertical coordinate at the gap entrance for a toroidal gap in the case of (a) reference (20°, 1 mm) and (b) ITER (5°, 0.5 mm).

4. Summary and conclusions

Plasma deposition is asymmetric in both poloidal and toroidal castellated tile gaps. Particle collection is a function of the dimension of the gap and the incidence of magnetic field lines. Strong electric fields developed along the sides of the gap govern the trajectories with the orientation of the magnetic field due to $\boldsymbol{E}\times\boldsymbol{B}$ drifts. In case of small poloidal gaps with grazing magnetic field lines, most of the incident ion flux is diverted over the entrance of the gap by the charge separation field and collected on the first millimeter of the leading edge of the downstream tile. This will lead to significantly enhanced local power loading (perhaps up to a factor of two), so these findings should be taken into account in thermomechanical modeling of the tiles. In the case of perfectly aligned toroidal gaps, practically all the flux that enters will impinge on the side favoured by the $\boldsymbol{E}\times\boldsymbol{B}$ drift. This finding is consistent with the observation that carbon layers form preferentially on the high field side of toroidal gaps on the bottom toroidal limiter in Tore Supra [12] ($\boldsymbol{B}$ is oriented in the negative toroidal direction). A small amount (10%) of the influx will be focused onto the leading corner of the tile face. This result might be different in the case of bevelled corners, and for slight misalignments of the gap with respect to the magnetic field; we will investigate these issues in the future.

Acknowledgements

The authors would like to thank Chantal Passeron for her useful technical support during the code development and Dr Vladimir Fuchs for helpful discussions. This work has been done under the Euratom Fellowship Contract No. 012801 (FU6).

References

[1] J. Schlosser et al., Nucl. Fus. 45 (2005) 512.
[2] W. Daener et al., Fus. Eng. Des. 61&62 (2002) 61.
[3] A. Litnovsky et al., J. Nucl. Mater. 337–339 (2005) 917.
[4] J.P. Gunn, Phys. Plasmas 8 (3) (2001) 1040.
[5] C.K. Birdsall, A.B. Langdon, Plasma Physics via Computer Simulation, McGraw-Hill, New York, 1985.

[6] W.H. Press et al., Numerical Recipes in Fortran, 2nd Ed., Cambridge University Press, 1992.
[7] O. Buneman, J. Comput. Phys. 1 (1967) 517.
[8] V. Fuchs et al., in: 32nd EPS Plasma Physics Conference, Tarragona, 2005.
[9] J.P. Gunn, J. Nucl. Mater. 337–339 (2005) 310.
[10] R. Chodura, Phys. Fluids 25 (1982) 1628.
[11] J.P. Gunn, Phys. Plasmas 4 (1997) 4435.
[12] C. Brosset, Private communication, 2006.